Novel physical sensors using evanescent microwave probes

Massood Tabib-Azar[a)]
Electrical Engineering and Computer Science Department and Macromolecular Science and Physics Departments, Case Western Reserve University, Cleveland, Ohio 44106

Deji Akinwande
Electrical Engineering and Computer Science Department, Case Western Reserve University, Cleveland, Ohio 44106

G. Ponchak
NASA Lewis Research Center, Cleveland, Ohio 44135

S. R. LeClair
Air Force Research Laboratory, Materials and Manufacturing Directorate, Wright-Patterson Air Force Base, Ohio 45433

(Received 24 March 1999; accepted for publication 26 April 1999)

Local probes, such as electron and photon tunneling, atomic force, and capacitance probes, are excellent sensing means for displacement and other related sensors. Here we introduce applications of a new local probe using evanescent microwave probe (EMP) in displacement sensing with a very high vertical spatial resolution (0.01 μm at 1 GHz), very high bandwidth (100 MHz), and stability. The EMP has been used in the characterization and mapping of the microwave properties of a variety of materials in the past and its application in gas sensing and thermography was recently explored and reported. The interesting feature of the EMP is that its characteristics can be easily altered for a specific sensing application by changing its geometry and frequency of operation. © *1999 American Institute of Physics.* [S0034-6748(99)04308-7]

I. INTRODUCTION

Many different sensors rely on the measurement of displacement and, in most cases, measuring displacement and force are closely related.[1] For example, by knowing the elastic properties of a structure, force can be calculated from the displacement measurement of that structure. Displacement sensors are the essential parts of many other more general sensors, as well. For example, displacement sensors can be used along with appropriate sensitive layers to sense gases and chemicals and their reactions.[2]

Different transduction methods can be used in sensing displacement. There are basically three categories of methods that may be used in *small* displacement sensors: (a) electrical, (b) magnetic, and (c) optical. Electrical methods include: (i) capacitive, (ii) piezoelectric, (iii) piezoresistive, (iv) tunneling current, and (v) evanescent microwave. Magnetic methods include: (i) magnetization methods, (ii) magnetoelastic methods, and (iii) external magnetic field methods.[1,3] Optical methods include two separate categories: (a) free-space methods and (b) guided-wave methods. Guided-wave methods can be further divided into fiber-optic and integrated-optic devices. Although acoustic methods can also be used as sensing means because of their relatively poor resolution, compared to the above methods, they are not used in displacement sensing.

The main objective of the present study is to introduce and discuss applications of the evanescent microwave methods in sensing displacements in the range 100 Å–5 mm. We have shown that the evanescent microwave probe (EMP) can be used in imaging microwave resistivity and nonuniformities in a variety of organic and inorganic materials including metals, semiconductors, insulators, and composites.[2–10] It is well known that evanescent fields can be used to resolve features smaller than the classical Abbe limit. Both evanescent optical waves and microwaves have been used in high-resolution imaging to resolve features several times smaller than the wavelength of radiation.[4–10] We have shown that it is experimentally possible to obtain a lateral resolution of around 0.4 μm at 1 GHz operation frequency[8] using a tapered microstripline resonator with a fine wire tip. This lateral spatial resolution was 200 times better than our first reported resolution.[4] According to our estimations, 0.01 μm resolution imaging using EMP operating at 10 GHz is possible.[7]

Evanescent fields are used in other frequency regimes as well.[1,3,11–14] Near-field scanning optical microscopes use evanescent fields to provide resolution on the order of 10–100 Å using light of 6000 Å wavelength. Atomic resolutions are achieved by using evanescent electron wave functions in scanning tunneling microscopy.

Evanescent microwave imaging methods compliment electronic and optical microscopes in the range of 0.01 μm–1 cm. Their main advantage is the ability to image subsurface features in poorly conducting materials, and to image bulk properties, due to greater penetration depth of microwaves, in insulators. Due to fast scan rates, and the possibility of using parallel probes, large-scale mapping of uniformities in materials can be performed by EMPs. Since it is a

[a)]Electronic mail: mxt7@po.cwru.edu

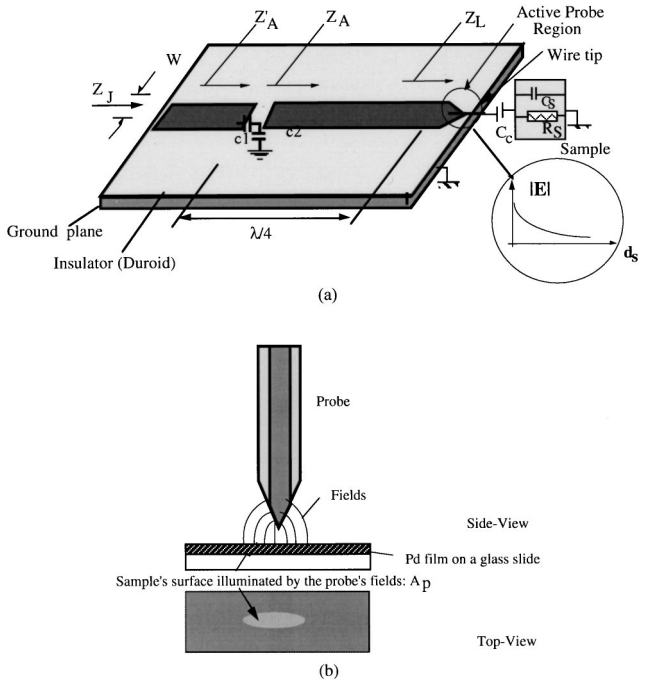

FIG. 1. (a) Microstripline resonator and probe assembly. Evanescent waves extend out of the tapered tip of the resonator. (b) Schematic of the probe–sample interaction area.

noncontact, noninvasive, and nondestructive method the EMP will also be very useful in the semiconductor fabrication environment.

Our research in evanescent microwave imaging has concentrated on using microstriplines (shown in Fig. 1), striplines,[7] and other two-dimensional waveguide structures[9] that have the following unique advantages. The resolution of the EMP can be engineered over a wide range by using different microwave substrate thickness and dielectric constants, tapering angles, feedline-to-resonator coupling strength, and various apertures in addition to frequency. We discuss some of these design parameters in Sec. II. Moreover, the planar EMP can be integrated with silicon micromachined parts to produce miniature parallel and compact probes.

II. OPERATION PRINCIPLES

EMP principles of operation are explained using a microstripline resonator geometry shown in Fig. 1(a). When an object is placed in the vicinity of the tip of the resonator [Fig. 1(b)], the resonator's reflection coefficient changes as shown in Fig. 2(a).[4–10] Both the resonance frequency f_r and the quality factor of the resonator Q are affected by the presence of the sample as can be clearly seen in Fig. 2(b).

The amount of change in the resonance (Δf_r and ΔQ) depends primarily on the microwave properties of the sample as well as on the distance between the resonator's tip and the sample d, and the tip's effective area A_{eff}.

Different signal detection methods can be used to monitor the microwave properties of a sample using an EMP.[7] As can be seen in Fig. 2(a), one can fix the operation frequency at f_x and monitor the change in the reflection amplitude. f_x is

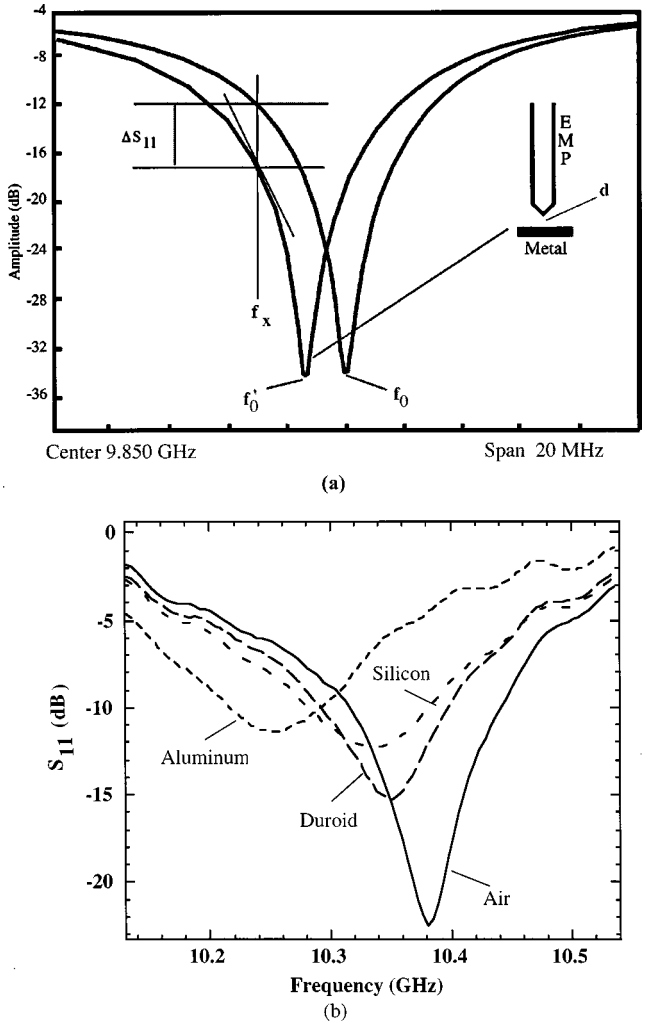

FIG. 2. (a) The EMP resonant frequency depends on the conductivity of samples placed near its tip. (b) In free space, the EMP has the highest resonant frequency; for an insulator (Duroid) sample, the EMP's resonant frequency becomes lower; for a metallic sample (aluminum), the EMP's resonant frequency becomes even lower.

usually chosen to yield maximum change in the probe's reflection coefficient for a given range of parameters in a sample.

Given a change in the reflection coefficient ΔS_{11} per a small change of Δd in the distance between a perfect conductor and the probe's tip, we can only detect ΔS_{11} if it is equal to or larger than the combined noise produced by the circulator/detector/amplifier circuit (Fig. 3). This requirement of signal to noise ratio of unity is an arbitrary requirement since it can be improved by using synchronous detection methods.[7]

As shown in Fig. 2(a), the detected signal ΔS_{11} can be related to the slope of the resonator at f_x (f_x is the operation frequency that is kept fixed throughout the measurement) using the following relationship:[2,7]

$$\Delta S_{11} \approx \left.\frac{\Delta S_{11}}{\Delta f}\right|_{f_x} \times \Delta f. \tag{1}$$

The slope $(\Delta S_{11}/\Delta f)_{f_x}$ is the sensitivity of the resonator at f_x and it will be denoted by S_x. Furthermore, the

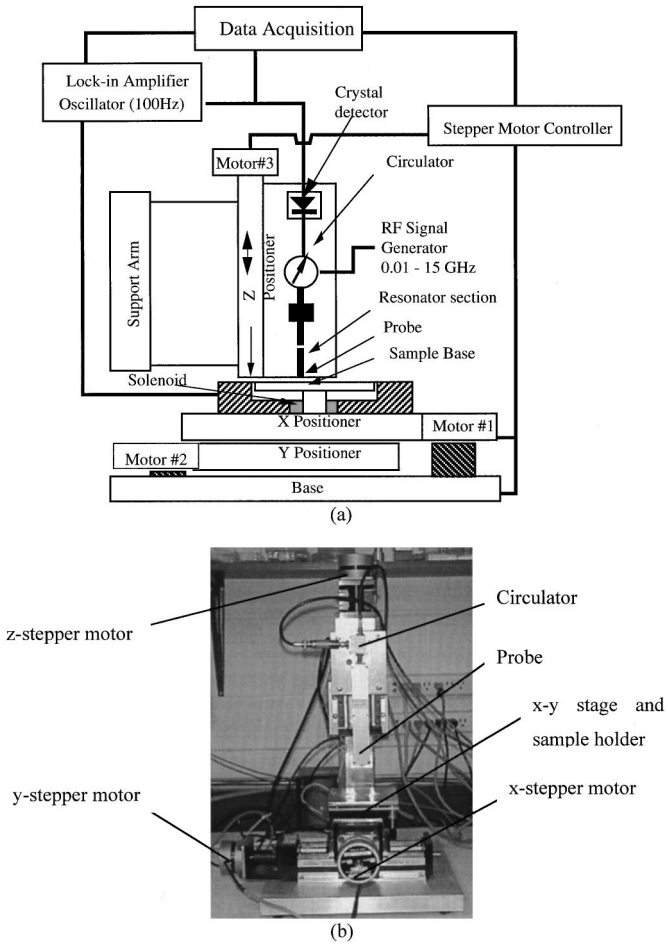

FIG. 3. (a) Schematic of the experimental setup. (b) The probe housing and the $x-y-z$ scanner arrangement.

minimum-detectable signal (MDS) is defined as the smallest change in the input (i.e., the measured) that produces an output ($\Delta V_{\text{out}}=\Delta S_{11}V_{\text{in}}$) equal to the rms value of the noise $V_{n\text{rms}}$. We note that in the case of conducting samples with large conductivities, ΔS_{11} can be written as $\Delta S_{11}/\Delta f=(\Delta S_{11}/\Delta d)(\Delta d/\Delta f)$. Thus, for MDS we can write

$$\Delta S_{11}=V_{n\text{rms}}/V_{\text{in}} \tag{2}$$

and

$$\text{MDS}=\Delta d=\frac{V_{n\text{rms}}/V_{\text{in}}}{S_x S_d}, \tag{3}$$

where S_d is $\Delta d/\Delta f$, and Δd is the smallest detectable change in the displacement. Equation (3) clearly shows that to improve MDS, both S_x and S_d should be maximized. S_x is related to the quality factor of the resonator, while S_d is determined by the physical interaction between the evanescent fields and the sample. S_d is the sensitivity of the probe.

Figure 1(b) schematically shows the interaction between the EMP and a sample located near its tip. The field patterns at the surface of the uniform sample are spread over an area denoted by $A_p \approx A_{\text{eff}}$, where A_p is the physical area of the tip and A_{eff} is an effective interaction area that is usually larger than A_p because of the fringing fields. If the sample moves toward the tip, the coupling increases and the probe's output changes accordingly. A similar change in the probe's output also occurs when the sample is nonuniform and its region of higher conductivity moves inside the probe's interaction region. Thus, it is important to differentiate between distance variations and variations in the microwave properties of the sample. In practice both the sample conductivity and probe-to-sample distance may change as the probe scans over the surface. Fortunately, the distance variation results in an exponential change in the probe's output while the sample nonuniformities usually occur over larger length scales.

TABLE I. Typical parameters of the EMP used in the present work.

A_p (cm^2)	d (μm)	L_0 (H)	C_c (pF)	f_0 (GHz)	C_0 (pF)	Q	$V_{n\text{rms}}$ (mV)	V_{in} (V)
6.4×10^{-5}	0.1	8×10^{-9}	8	1	3.18	1000	20	10

The interesting aspect of our approach, as given in Eq. (3), is that the internal probe characteristic (given by S_x) can be completely separated from the external probe interaction (given by S_d). To calculate S_d we note that the resonator's quality factor in the presence of an external object Q' is given by $1/\omega_0' C_0' R_0'$, where ω_0' is the resonance radial frequency of the perturbed probe, C_0' is an equivalent capacitance of the resonator, and R_0' is its equivalent resistance. These parameters are extensively discussed in Ref. 7. Using the relationship between Q', we can solve for the resonance frequency f_0':

$$f_0'=\frac{1}{2\pi R_0' C_0' Q'}. \tag{4}$$

Next we use Eqs. (10b) and (13) in Ref. 7 for C_0' and R_0':

$$C_0' \approx C_0+C_c \tag{5}$$

and for a highly conducting sample where its surface resistance R_s is very small,

$$R_0' \approx R_0+R_s C_c \omega^2 (C_c-C_0) \approx R_0. \tag{6}$$

The coupling capacitance C_c is approximately given by

$$C_c=\frac{\epsilon_0 A_{\text{eff}}}{d}. \tag{7}$$

Using the above equations, S_d can be calculated as

$$S_d=\frac{\epsilon_0 A_{\text{eff}} f_0}{d(C_0 d+\epsilon_0 A_{\text{eff}})}. \tag{8}$$

Using typical values shown in Table I, it can be seen that $C_0 d > \epsilon_0 A_{\text{eff}}$. Thus, S_d becomes

$$S_d \approx \frac{\epsilon_0 A_{\text{eff}} f_0}{C_0 d^2}=\frac{8.854\times10^{-14}\times6.4\times10^{-5}\times10^{10}}{3.18\times10^{-12}\times10^{-6}}$$
$$=1.8\times10^{10}. \tag{9}$$

It is interesting to note that S_d has a d^{-2} dependence on the distance between the probe tip and the sample. This is in contrast with most of our published work that indicates an exponential dependence on distance when the tip is very near the conducting sample. The main reason for this apparent discrepancy is the approximate analytical form of the C_c that is given in Eq. (7). The contribution of the fringing fields to

the coupling capacitance of the EMP is discussed in Ref. 7 and they are also discussed in Ref. 4 for more general cases.

Assuming that the resonator is matched to the characteristic impedance of the feedline at resonance frequency (i.e., $R_0' \approx Z_0$ at $\omega = \omega_0'$), as shown in Ref. 7, $S_x (= dS_{11}/df|_{f_x})$ is given by

$$S_x \approx s \frac{\sqrt{2}Q'}{\omega_0'} \left(1 - \frac{\Delta\omega}{\omega_0'}\right) \approx s \frac{\sqrt{2}Q}{\omega_0} \left(1 - \frac{\Delta\omega}{\omega_0}\right), \tag{10}$$

where $\omega = \omega_0 + \Delta\omega$ and $\Delta\omega/\omega_0 \ll 1$ and $s = -1$ if $\omega < \omega_0$ and $s = +1$ if $\omega > \omega_0$. Thus, the sensitivity is proportional to the quality factor of the resonator, as expected.

For the EMP used in our work, $Q \approx 1000$ at $\omega_0 = 2\pi \times 10^{10} = 6.28 \times 10^{10}$ and $S_x \approx 2.25 \times 10^{-7}\,(\mathrm{s}^{-1})$ for $\Delta\omega/\omega_0 \ll 1$. Typical probe parameters are given in Table I.

Using Eqs. (9) and (10) along with (3), the MDS becomes

$$\mathrm{MDS} = \Delta d = \frac{V_{n\mathrm{rms}}}{V_{\mathrm{in}}} \frac{2\pi d(C_0 d + \epsilon_0 A_{\mathrm{eff}})}{Q(1 - \Delta f/f_0)\epsilon_0 A_{\mathrm{eff}}}. \tag{11}$$

For typical values of S_d and S_x, respectively, given in Eqs. (9) and (10), we find a typical numerical value for MDS:

$$\mathrm{MDS} = \Delta d \approx \frac{V_{n\mathrm{rms}}}{V_{\mathrm{in}}} \frac{2\pi d(C_0 d)}{Q(1 - \Delta f/f_0)\epsilon_0 A_{\mathrm{eff}}} = 0.025\,\mu\mathrm{m}. \tag{12}$$

In regions where S_{11} exhibits exponential dependence on distance, the resonance frequency can be written as $f_0' = f_0 + \delta f$ with δf given by

$$\delta f = C(f, \sigma)\epsilon^{-\xi d}, \tag{13}$$

where σ is the conductivity of the cantilever beam at the probe frequency and C is a coefficient that is a function of σ and f, and ξ is the effective decay length of the evanescent field at the tip of the probe. Thus the probe sensitivity S_d is given by

$$S_d = -\xi C(f, \sigma) e^{-\xi d}. \tag{14}$$

Furthermore, S_{11} can be approximately written by

$$S_{11} = (1 - e^{-(f - f_0)^2/(\Delta f)^2}), \tag{15}$$

where Δf is the bandwidth of the resonator. Thus, the resonator's sensitivity S_x is given by

$$S_x = \frac{2(f_0 - f)}{(\Delta f)^2}(1 - S_{11}). \tag{16}$$

Using Eqs. (13) and (16) along with (3), we find the following MDS:

$$\mathrm{MDS} = \Delta d = \frac{V_{n\mathrm{rms}}}{V_{\mathrm{in}}} \frac{(\Delta f)^2 e^{\xi d}}{2\xi C(f, \sigma)(f - f_0)(1 - S_{11})}. \tag{17}$$

Typically $(1 - S_{11}) \approx 0.5$, $f - f_0 \approx \Delta f/2$, $C(1\,\mathrm{GHz}, 10^8\,\mathrm{S}) \approx 2.2 \times 10^6\,\mathrm{MHz}$, $\xi = 1/10\,\mu\mathrm{m}^{-1}$, $d = 10\,\mu\mathrm{m}$, $V_{\mathrm{in}} \approx 20\,\mathrm{V}$, and $V_{n\mathrm{rms}} \approx 20\,\mathrm{mV}$. Thus, for these typical values, MDS becomes

$$\mathrm{MDS} = \Delta d = 4.5 \times 10^{-4} \frac{e^{\xi d}}{\xi} \approx 0.01\,\mu\mathrm{m}. \tag{18}$$

It is interesting to note that both Eqs. (12) and (18) result in a similar MDS values. This is mainly because for $d \approx \xi^{-1} \gg 0$, the $1/d^2$ dependence of Eq. (9) and $e^{-\xi d}$ dependence of Eq. (14) are similar. The circuit approach that is used in defining the coupling capacitance is only an approximation and it does not account for the decay of electromagnetic fields near the tip. Using the electromagnetic calculations we have shown that ξ^{-1} of theses fields directly scales with frequency and ξ^{-1} becomes shorter at higher frequencies.

III. EXPERIMENTAL RESULTS AND DISCUSSIONS

The experimental setup is shown in Fig. 3 and it is similar to the setup previously reported.[3–13] It consists of a microwave resonator coupled to a feedline [Fig. 1(a)] and connected to a circulator. The circulator is also connected to a 0.01–15 GHz signal generator, and to a crystal microwave detector. The detector output is a dc voltage proportional to the magnitude of the reflected wave. This voltage is fed to an amplifier and subsequently to a lock-in amplifier. The probe is mounted vertically over an $x-y$ stage. Both the $x-y$ stage and the frequency generator are controlled by a computer that also acquires data from the lock-in amplifier. In synchronous measurements, either the probe or the sample, are vibrated at ≈100 Hz.

Transduction speed, resolution, and drift are the main parameters of importance in the displacement sensors. Packaging, cost, and other more practical considerations are also important but they lie beyond the scope of the work presented here.

The transduction bandwidth in our case was limited to 1 kHz by the lock-in amplifier used to perform the synchronous detection of the EMP signal and it can be increased to 100 MHz by using a faster lock-in amplier or by changing the detection electronic.

To use the EMP as a displacement sensor, it is essential to examine how its resolution is affected by the geometry of its resonator. First, the EMP's resonator can be constructed using different microwave substrates with different dielectric constants and thickness. Second, the strength of coupling between the resonator and the feedline can be chosen to result in undercoupling, critical coupling, or overcoupling. Third, the resonator tip can be tapered with different angles and a wire tip can be attached to the tapered region to further improve the EMP's resolution.

The effect of substrate parameters and coupling strength on the EMP resolution are discussed previously and it is shown that the critical coupling results in the shortest field decay length near the EMP's tip.

The change in the EMP's output as a function of the tip-to-sample distance d shown in Figs. 4 and 5. ξ^{-1} in these cases ranged from 2 μm to 4 mm. ξ depends on the operation frequency, the tapering angle of the resonator [see Fig. 1(a)], the length and diameter of the wire tip attached to the resonator, the resonator's substrate dielectric constant and thickness, and the coupling strength between the resonator and the feedline section. All these parameters are shown in Fig. 1(a) and they are discussed in Refs. 4–9. Thus, even without

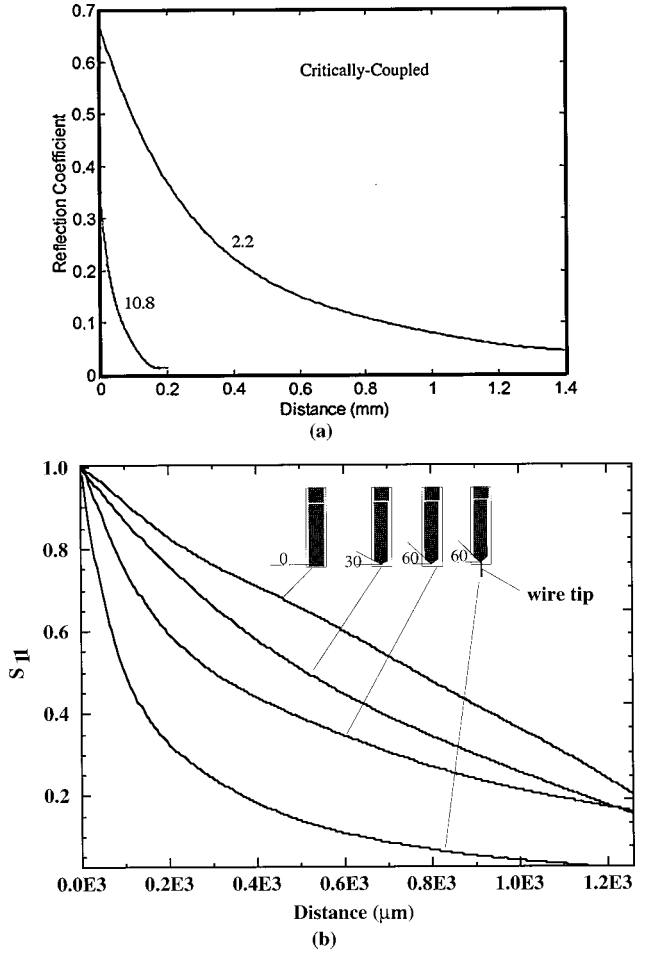

FIG. 4. (a) Comparison of decay characteristic lengths for critically coupled EMP on Duroid with two different permittivities. (b) The effect of tapering angle and a wire tip on the decay length.

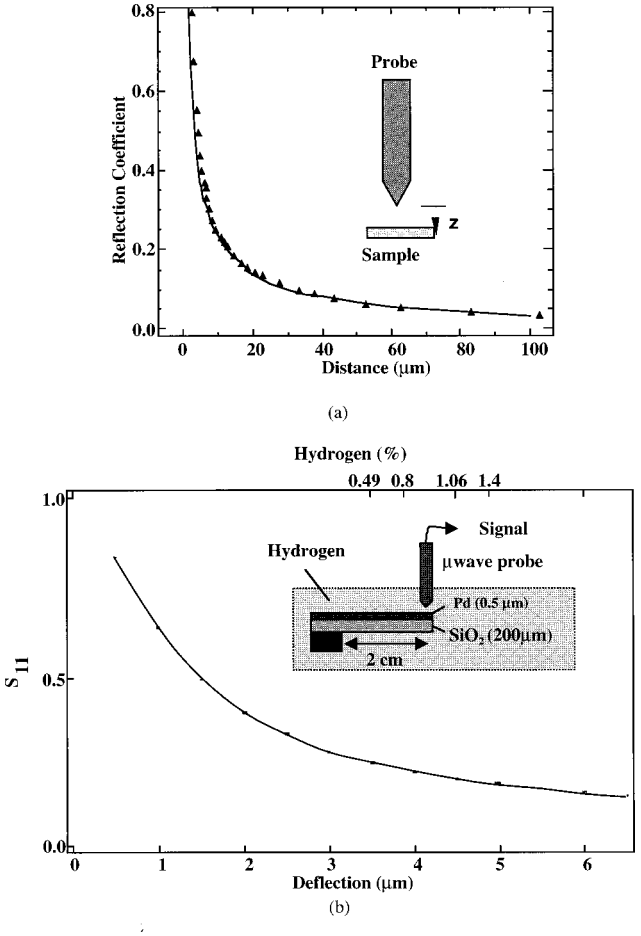

FIG. 5. (a) S_{11} of a 10 GHz EMP with a wire tip and 60° tapering on a Duroid substrate of 10.8 relative permittivity. (b) Deflection of a palladium coated cantilever beam exposed to hydrogen and detected by an EMP at 1 GHz.

changing the operation frequency it is possible to vary the distance sensitivity of the probe over a wide range.

Figure 4(a) shows the effect of the substrate permittivity on the characteristic decay of the fields near the EMP's tip. All the resonators we used in our probes had 50 Ω characteristic impedance and, hence, larger permittivity substrates were thinner and they resulted in shorter decay lengths [Fig. 4(a)].

The effect of the tapering angle is shown in Fig. 4(b) for a 10 GHz EMP with a dielectric substrate of 3.8 relative permittivity. The untapered tip (0°) had the longest ξ^{-1} of 2 mm. ξ^{-1} monotonously decreased as the tapering angle was increased and it was 300 μm at 60°. A ξ^{-1} of 100 μm was obtained using a wire tip attached to the 60° tapered probe as can be seen in Fig. 4(b). The decay length was further reduced to 4 μm by using a dielectric substrate of 10.8 relative permittivity as shown in Fig. 5(a). The MDS in this case was 0.1 μm. Although, not of interest in the present application, the wire tip also significantly improves the lateral resolution of the EMP.

The main question is how the tapering of the probe's tip or attaching a wire reduces ξ^{-1}? This can be seen by noting that as the EMP tip is tapered the fields become more concentrated and confined near the apex. The lateral confinement of the fields also reduces their extension in the z direction, hence, reducing ξ^{-1}.

As we mentioned in the beginning of this article, displacement sensing is used in a variety of other sensors including gas sensors. To illustrate this point, Fig. 5(b) shows the application of the EMP in detecting deflection of a palladium coated cantilever beam that was exposed to hydrogen. It is well known that palladium absorbs hydrogen and as a result its volume expands. The expansion in the volume of a thin-film palladium deposited over a compliant substrate such a cantilever beam, results in the bending of the cantilever beam. The amount of the bending depends on the Young modulus of the substrate and the thin film, thickness, and dimensions of different layers, as well as on the stress between layers. The stress between the Pd film and the canti-

TABLE II. Deflections d of the Pd-coated cantilever beam and calculated stress and strain ($\epsilon=\sigma/Y$) in the Pd film as a function of hydrogen concentrations. Strain of a bulk Pd is also given.

H_2 conc. (%)	Deflection, d (μm)
0.49	3.0
0.80	3.9
1.07	4.5
1.41	4.9

lever beam depends on the amount of hydrogen absorbed by Pd. In Ref. 2 we show how the Pd-coated cantilever beam's deflection, detected by the EMP, can be used to monitor the hydrogen concentration. The numerical values of the cantilever beam deflection at various hydrogen concentration levels are shown in Table II.

[1] A. Garcia and M. Tabib-Azar, Sens. Actuators A **48**, 87 (1995).
[2] M. Tabib-Azar, B. Sutapun, and R. Muller, Rev. Sci. Instrum. (submitted).
[3] M. Tabib-Azar, *Integrated Optics and Microstructure Sensors* (Kluwer Academic, Boston, 1995).
[4] M. Tabib-Azar, N. S. Shoemaker, and S. Harris, Meas. Sci. Technol. **4**, 583 (1993).
[5] P. Pathak, M. Tabib-Azar, and G. Ponchak, 1998 Conference of Non-Destructive Testing, Anaheim, CA, 1998.
[6] M. Tabib-Azar, P. S. Pathak, G. Ponchak, and S. R. LeClair, Rev. Sci. Instrum. **70**, 2783 (1999).
[7] M. Tabib-Azar, G. Ponchak, and S. LeClair, Rev. Sci. Instrum. (to be published).
[8] M. Tabib-Azar, D.-P. Su, A. Pohar, and S. L. LeClair, Rev. Sci. Instrum. **70**, 1725 (1999).
[9] G. E. Ponchak, A. Akinwande, M. Tabib-Azar, and S. R. LeClair, Microwave Theory and Techniques Symposium, 1999 (accepted for publication).
[10] M. Tabib-Azar, R. Ciocan, G. Ponchak, and S. R. LeClair, Rev. Sci. Instrum. (to be published).
[11] D. Sarid, *Scanning Force Microscopy* (Oxford University Press, New York, 1991), pp. 55–64.
[12] M. F. Bocko, K. A. Stephenson, and R. H. Koch, Phys. Rev. Lett. **61**, 726 (1988).
[13] K. Stephenson, M. F. Bocko, and R. H. Koch, Phys. Rev. A **40**, 6615 (1989).
[14] M. F. Bocko, Rev. Sci. Instrum. **61**, 3763 (1990).